Excess specific heat from the gapped sliding phonon modes in the incommensurate composite crystal $Sr_{14}Cu_{24}O_{41}$

Rabindranath Bag,[1] Soumitra Hazra,[2] Rajeev N. Kini,[2] and Surjeet Singh[1,*]
[1]*Indian Institute of Science Education and Research, Pune 411008, Maharashtra, India*
[2]*Indian Institute of Science Education and Research, Thiruvananthapuram 695551, Kerala, India*

(Received 15 August 2018; published 13 February 2019)

We show that the low-temperature specific heat (C_p) of the incommensurate chain-ladder system $\{CuO_2\}_\alpha\{Sr_2Cu_2O_3\} = Sr_{14}Cu_{24}O_{41}$ (for $\alpha = 10/7$) shows a rather large excess contribution of nonmagnetic origin. Diluted Al doping at the Cu site or annealing the crystal in an O_2 atmosphere suppresses this feature considerably. Using THz time-domain spectroscopy, we relate the occurrence of excess specific heat to the presence of very low-energy (∼1 meV) gapped phonon modes that originate from the sliding motion of oppositely charged $\{CuO_2\}$ chain and $\{Sr_2Cu_2O_3\}$ ladder sheets past each other.

DOI: 10.1103/PhysRevB.99.054305

I. INTRODUCTION

Crystalline materials, regardless of their composition and symmetry properties, exhibit a universal phononic ground state consisting of three gapless acoustic modes whose contribution to the specific heat is well known to vary as the Debye T^3 law [1]. However, in a composite crystal comprising two substructures that individually obey *full* translational symmetry but are mutually incommensurate (IC) along one or more directions, the phononic ground state can be highly unconventional due to the occurrence of new normal modes that arise from a relative sliding motion of these substructures past each other [2–5]. An "extra" acoustic or acousticlike mode has indeed been observed experimentally in a number of IC systems, including the IC chain compound $Hg_{3-x}AsF_6$ [6,7], higher manganese silicides of the Nowotony chimney-ladder family [8], Rb-IV [9], *n*-alkane-urea composite crystals [10], and in some of the BSCCO superconductors [11,12]. Within this, a particularly interesting behavior emerges when the IC substructures are in the form of oppositely charged sheets as the Coulomb restoring force between these sheets, as they slide past each other, opens an energy gap rendering the sliding mode quasiacoustic or optical [13]. Such systems are interesting as they not only offer a tunable phonon gap that scales with the charge difference between the sliding layers, but they also provide a platform for understanding the gapped phononic excitations in a wider class of systems, including disordered solids and glasses [14–16], filled skutterudites [17], and strong electron-phonon coupling superconductors [18].

In this regard, the composite crystal $\{CuO_2\}_\alpha\{Sr_2Cu_2O_3\}$ is an ideal system for realizing the gapped sliding modes. It has a layered structure comprising an alternating stack of oppositely charged $Sr_2Cu_2O_3$ and CuO_2 sheets. In the $Sr_2Cu_2O_3$ sheet, the Cu ions form a network of weakly interacting two-leg ladders running parallel to the *c*-axis, and in the CuO_2 sheet they arrange to form linear chains oriented parallel to the *c*-axis (Fig. 1). These sheets are, however, mutually IC along the *c*-axis with $\alpha = c_l/c_c \approx \sqrt{2} \approx 10/7$, where c_c (∼2.75 Å) and c_l (∼3.93 Å) are the lattice parameters in the chain and ladder sublattices, respectively. In real materials, α exhibits a broad distribution of values, which is the hallmark of any IC system [19]. This is also reflected in the high-energy x-ray diffraction study where not a single ordering wave vector but a multitude of Fourier components characterize the low-temperature modulations of the chain sublattice [20]. For brevity, however, in the rest of the manuscript we will use the notation "$Sr_{14}Cu_{24}O_{41}$," which corresponds to $\alpha = 10/7$.

While the magnetic ground state and spin excitations of $Sr_{14}Cu_{24}O_{41}$ have been investigated extensively in the past [21], the unconventional nature of its phononic ground state started gaining attention only recently. Thorsmølle *et al.* [22] used terahertz time-domain spectroscopy (THz-TDS) and Raman techniques to show the occurrence of new infrared and Raman active modes in the very low0energy range between 1 and 2 meV. They conjectured that these modes arise due to the gapped sliding motion of the chain and ladder layers. More recently, new optical phonon modes polarized along the incommensurate axis were reported in the same energy range using inelastic neutron scattering [23]. However, the thermodynamic evidence of these modes and their unambiguous assignment as the sliding phonon modes has remained an open question.

Since the sliding modes are expected to be gapped, they should have a definitive thermodynamic signature in the low-temperature specific heat (C_p) where the phononic contribution is expected to exceed the Debye T^3 prediction. In this paper, we show that the low-temperatures specific heat (C_p) of $Sr_{14}Cu_{24}O_{41}$ exhibits a rather large excess contribution of nonmagnetic origin near $T^* = 10$ K. Using a combination of THz-TDS and specific-heat experiments on three different crystals, namely as-grown, O_2-annealed, and Al-doped, we establish that the excess specific heat in $Sr_{14}Cu_{24}O_{41}$

*surjeet.singh@iiserpune.ac.in

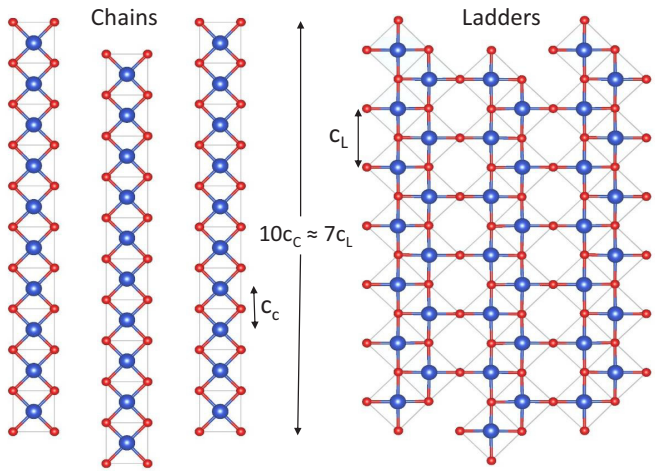

FIG. 1. The chain (CuO_2) and ladder ($Sr_2Cu_2O_3$) sublattices. Blue and red spheres represent Cu and O ions. The Sr ions are not shown for clarity.

originates from the relative sliding motion of chain and ladder layers predicted previously. We also show that the gap size associated with these modes is highly sensitive to the stoichiometry.

II. EXPERIMENTAL DETAILS

Our experiments are performed on high-quality single crystals grown using the traveling-solvent floating-zone technique. The details of crystal growth and structural characterizations are given in Ref. [24]. All the crystals were grown under similar conditions of 3.0 ± 0.2 bar oxygen pressure and a growth rate of $1.0 \pm 0.2\,\mathrm{mm\,h^{-1}}$. The annealing treatment was carried out in a tubular furnace under flowing O_2 at $T = 850\,^{\circ}\mathrm{C}$ for 36 h. The quality of grown crystals was analyzed using several complementary techniques, including powder x-ray diffraction, polarized-optical and scanning electron microscopies, and the x-ray Laue technique. An accurate compositional analysis of the Al-doped crystal was done using the inductively coupled plasma–atomic emission spectroscopy (ICP-AES) method. Magnetic and specific heat measurements were performed using a physical property measurement system (PPMS), Quantum Design (QD), USA. For the specific-heat measurements, thin, plateletlike specimens with their largest surface area parallel to the *ac*-plane were mounted on the specific heat puck using Apiezon N grease. Prior to loading the specimen, addenda were measured to subtract the specific heat of the sample holder and of grease used during the experiment. For THz-TDS experiments, the THz signals were generated using ultrafast (~80 fs) photoexcitation of low-temperature grown GaAsBi epilayers, and they were detected using a photoconductive antenna. Measurements were performed by mounting the sample on the cold finger of an optical closed-cycle refrigerator. Transmittance was obtained by taking the ratio between the magnitude of the fast-Fourier transformed sample and the reference amplitudes.

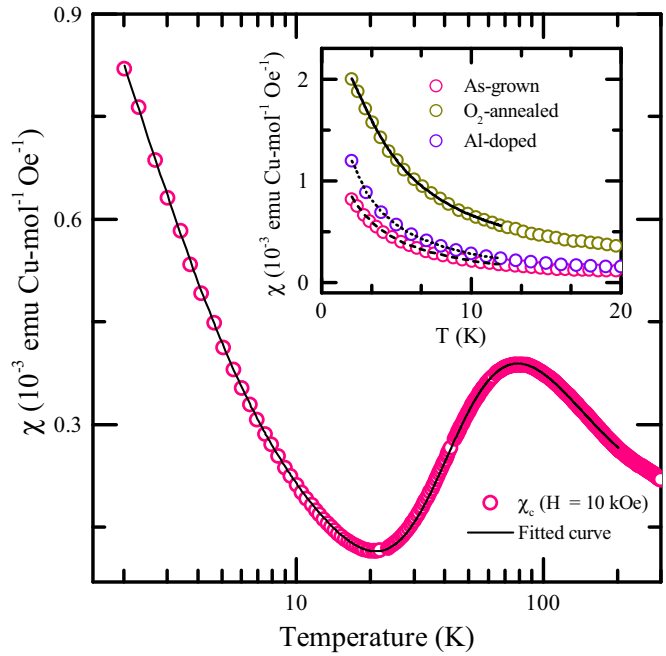

FIG. 2. Magnetic susceptibility χ of $Sr_{14}Cu_{24}O_{41}$ is shown as a function of temperature for H ∥ c. The black line represents the best fit to the data obtained using Eq. (1). Inset: low-temperature χ for an as-grown, annealed, and Al-doped crystal. The lines are best fit to the data using Eq. (1) in the low-temperature range as described in the text.

III. RESULTS AND DISCUSSION

A. Magnetic susceptibility

The temperature dependence of spin susceptibility (χ) for H ∥ *c* is shown in Fig. 2. Since the ladder sublattice has a spin-singlet ground state with the singlet-triplet energy gap exceeding ~35 meV [25,26], the low-temperature χ is practically due to the chain sublattice. $Sr_{14}Cu_{24}O_{41}$ is self-hole doped with six holes per formula unit. If all six holes are assumed to be present in the chain subsystem, the ground-state configuration of the chains can be written as follows [27]: $\cdots \circ \circ [\uparrow \circ \downarrow] \circ \circ [\downarrow \circ \uparrow] \circ \circ \cdots$, where $\uparrow$ ($\downarrow$) represents a Cu^{2+} spin 1/2, $\circ$ represents a Zhang-Rice singlet [28], and $[\uparrow \circ \downarrow]$ denotes a spin-1/2 dimer. For this ideal configuration, χ should decrease to zero exponentially as $T \to 0$. However, in any real $Sr_{14}Cu_{24}O_{41}$ crystal, a small fraction of hole transfer from chains to ladders leads to a small number of unpaired spins in the chains that cause $\chi(T)$ to increase at low temperatures ($T < 20\,\mathrm{K}$) in a Curie-like manner. Recently, it has been shown that at still lower temperatures ($T < 5\,\mathrm{K}$), these unpaired spins, separated by hundreds of Cu sites along the chain, antialign to form dimers due to a small antiferromagnetic interaction mediated via the intervening sites [29]. Therefore, χ below $T = 200\,\mathrm{K}$ can be described using a dimer-dimer model represented by Eq. (1):

$$\chi = \chi_0 + \frac{2N_A g^2 \mu_B^2}{k_B T} \sum_i \frac{N_{d_i}}{\left(3 + e^{-\frac{J_i}{k_B T}}\right)} + \frac{C}{T}, \qquad (1)$$

where χ_0 ($\sim 10^{-5}$ emu/mol) represents a small temperature-independent van-Vleck contribution; the second term is the

TABLE I. The fitting parameters for the as-grown, O_2-annealed, and Al-doped crystals using Eqs. (1) and (2). In $\chi(T)$ fits, N_s is obtained from the Curie constant C, and in the C_p fits from the coefficient A of the AT^{-2} term. The value of β was fixed by first fitting the measured C_p in the temperature range $T = 12$ to 15 K using the expression $C_p = C_0 + \beta T^3$, where C_0 is some constant.

	Susceptibility (χ)				Specific heat (C_p)			
Sample	N_{d2} (f.u.$^{-1}$)	J_2 (K)	$\chi_0(10^{-5})$ (emu Cu-mol^{-1} Oe^{-1})	N_s (f.u.$^{-1}$)	N_{d2} (f.u.$^{-1}$)	J_2 (K)	β (mJ mol^{-1} K^{-4})	N_s (f.u.$^{-1}$)
As-grown	0.04	4.3	−3.0	0.08	0.06	2.7	5.3	0.13
O_2-annealed	0.16	4.0	−1.2	0.12	0.16	2.0	5.8	0.29
Al-doped	0.045	3.5	−2.8	0.10	0.05	4.5	5.4	0.04

chain dimer susceptibility, where $i = 1$ represents the dimers [↑ ∘ ↓], and $i = 2$ represents the long-distance dimers described above. N_A denotes the Avogadro number, g is the Landé factor; μ_B is the Bohr magneton, and k_B is the Boltzmann constant; N_{d_i} denotes the number of dimers per formula unit (f.u.), and J_i is the intradimer coupling. The last term in Eq. (1) represents the Curie contribution due to the spins that remain undimerized down to $T = 2$ K.

As shown in Fig. 2, a satisfactory fit to $\chi(T)$ over a broad temperature range is obtained using Eq. (1). The best-fit value of J_1 and J_2 is about 132 and 2 K, respectively, in good agreement with previous reports (see Ref. [30] for J_1 and Ref. [29] for J_2). The number of free spins N_s, calculated from C, is ∼0.069/f.u., and N_{d1} and N_{d2} are 1.89/f.u. and 0.04/f.u. respectively. Here, however, our interest is primarily in obtaining the low-temperature parameters: N_s, N_{d2}, J_2 in Eq. (1), and to compare these to a similar fitting for the low-temperature specific heat (*vide infra*). Therefore, in Fig. 2 (inset) we show $\chi(T)$ for as-grown, O_2-annealed, and Al-doped crystals along with the corresponding low-temperature fits, where the fits are performed using Eq. (1) after excluding from it the high-temperature $i = 1$ dimer term whose contribution at low temperatures ($T \lesssim 20$ K) becomes exceedingly small. The values of the fitting parameters thus obtained are summarized in Table I. For a more elaborate discussion on the analysis of $\chi(T)$ using various models, including Eq. (1), we refer the reader to Ref. [31].

B. Specific heat

The main result of our paper is shown in Fig. 3, where the specific heat (C_p) is shown as a function of temperature for the as-grown crystal. When plotted as C_p versus T (not shown), the data, otherwise smooth down to 2 K, showed a slight blip near $T^* = 10$ K. This feature becomes clearly discernible in the C_p/T versus T^2 (panel a), where data in the presence of an applied magnetic field of 50 kOe are also shown. The small difference between the zero-field and in-field data is due to the presence of a small fraction of free or defect spins in the chains. As the sample is cooled, these spins tend to align along the field direction, thus giving rise to a small excess field-dependent contribution. At still lower temperatures, a gradual onset of long-distance dimerization takes place that leads to a magnetic-field-dependent upturn in C_p/T. Both of these contributions should be subtracted from the measured C_p in order to examine whether the $T^* = 10$ K feature, which has no counterpart in $\chi(T)$, has any field dependence or not. For this purpose, the low-temperature data in the temperature range from $T = 2$ to 3 K, which is sufficiently away from T^*, are fitted using the following expression:

$$C_p(T) = RN_{d_2}(J_2/k_BT)^{\frac{3}{2}}e^{-J_2/k_BT} + \beta T^3 + AT^{-2}, \quad (2)$$

here the first term is due to the long-distance dimers, where R is the gas constant, βT^3 is the phononic contribution, and the term A/T^2 represents the Schottky tail due to a small number of unpaired spins, i.e., the spins that remain undimerized down to 2 K. The fitted curve [shown in Fig. 3(b), where C_p is plotted as C_p/T^3 versus T] is extrapolated to higher temperatures. The values of parameters N_{d2}, J_2, and A are summarized in Table I, and they are in good agreement with corresponding values obtained from the $\chi(T)$. The value of β is found to be ∼5.5 J mol^{-1} K^{-4} in agreement with a previous report in which C_p at low temperatures is reported [32].

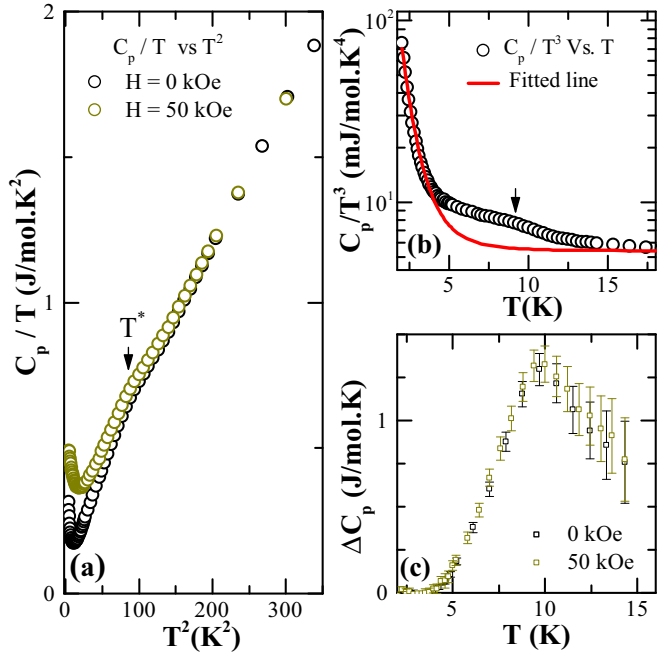

FIG. 3. (a) Specific heat (C_p) of an as-grown $Sr_{14}Cu_{24}O_{41}$ crystal plotted as C_p/T vs T^2 in zero-field, and under a field of 50 kOe; (b) C_p/T^3 is shown as a function of T. The solid black line is a fit in the range $T = 2$–3 K using Eq. (2) (see text for details); (c) ΔC_p is plotted as a function of temperature for $H = 0$ and 50 kOe. The error bars are taken directly from the PPMS data file.

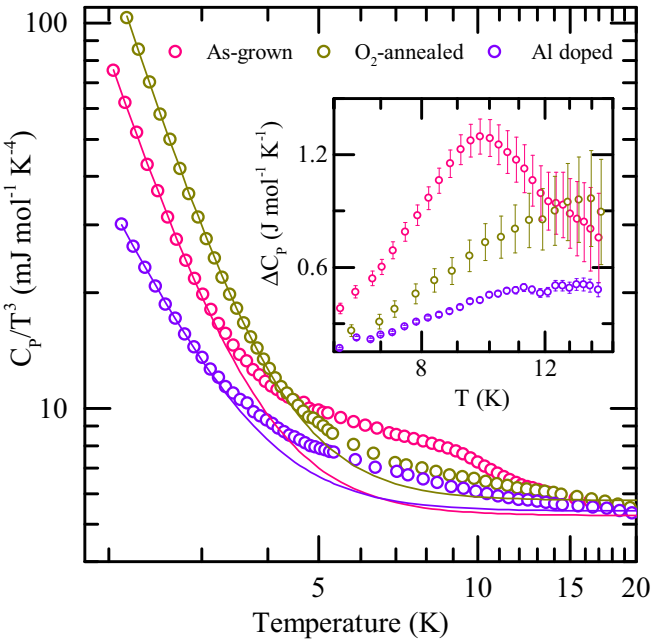

FIG. 4. Specific heat (C_p) of as-grown, O_2-annealed, and Al-doped crystals shown as a function of temperature in the C_p/T^3 representation. The solid lines in the main panel are the fitted lines that are extrapolated for $T > 3$ K. In the inset, ΔC_p is plotted as a function of temperature (see the text for details). The error bars are taken directly from the PPMS data file.

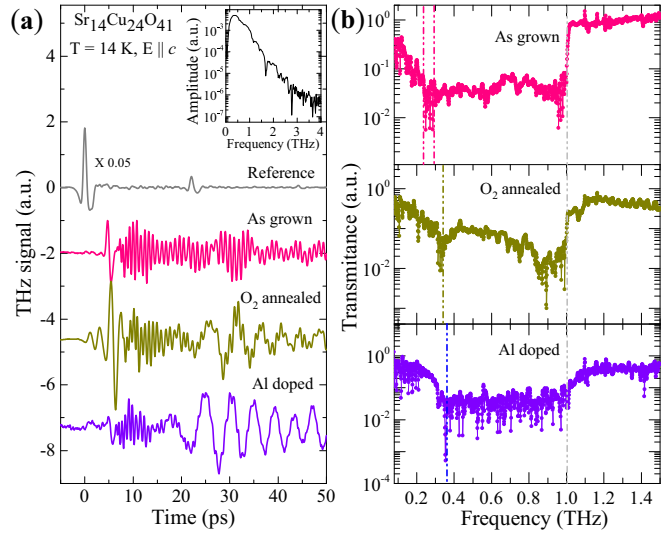

FIG. 5. (a) Transmitted THz electric field (E) at $T = 14$ K, and for $E \parallel c$; (b) THz transmittance for $E \parallel c$ at $T = 14$ K for the as-grown, oxygen-annealed (O_2 ann), and Al-doped $Sr_{14}Cu_{24}O_{41}$ crystals. The inset in the left panel shows the fast-Fourier transform amplitude spectrum of the THz electric field for the reference.

The excess specific heat (ΔC_p), estimated by taking the difference between the experimental data and the fitted curve, is shown in the inset of Fig. 3(c) for $H = 0$ and 50 kOe. ΔC_p exhibits a well-defined peak at T^*, whose nonmagnetic or phononic origin can be inferred from the insensitivity of ΔC_p to the applied magnetic field, which also agrees with the absence of any anomalous feature in $\chi(T)$ at or around T^*. The peak height exceeds 1 J mol^{-1} K^{-1} at T^*, which is rather large given its nonmagnetic origin. A comparable excess C_p was previously reported in the pyrochlore $Bi_2Ti_2O_7$ where the quenched configurational disorder among the Bi lone pairs results in a departure from the Debye T^3 law [33].

In Fig. 4, C_p is shown for the O_2 annealed and 0.25% Al-doped crystals; the corresponding data for as-grown crystal are also included for comparison. Below $T \approx 4$ K, where the long-distance dimerization of the unpaired spins is expected to set in, C_p is enhanced due to O_2 annealing but suppressed for Al doping. However, in both O_2 annealed and Al-doped crystals, C_p exhibits a strong suppression in the region around T^*, which is what we are primarily interested in. The measured C_p of annealed and Al-doped crystals is also fitted using Eq. (2) to extract ΔC_p. The fitted curves are also shown in Fig. 4. In the inset, estimated ΔC_p is shown. In both cases, the phononic anomaly in ΔC_p decreases in magnitude and shifts toward higher temperatures. A similar departure from T^3 behavior was also observed by Chen *et al.* [23]. However, the 10 K anomaly in their data is hugely suppressed, which may be related to the fact that C_p of $Sr_{14}Cu_{24}O_{41}$ in the range $T < 15$ K is highly sensitive to the growth conditions and post-growth annealing treatment as shown here (see also the Appendix). To investigate this further, we carried out THz-TDS of all three specimens, which is presented next.

C. Terahertz spectroscopy (THz)

In Fig. 5(a), the THz signal transmitted through the sample is shown for the as-grown, oxygen-annealed, and Al-doped crystals at $T = 14$ K and with electric field (**E**) polarized along the c-axis ($E \parallel c$). The reference signal without the sample is also shown. The THz electric field of the as-grown crystal can be broadly characterized by the presence of two types of oscillations having periods ∼1 and ∼4 ps. For $E \parallel a$ (not shown) the THz signal showed no oscillations, in agreement with the data reported earlier by Thorsmølle *et al.* [22]. As shown in Fig. 5, for $E \parallel c$ the annealed and doped crystals show a significantly different behavior compared to the as-grown crystal. To assess this difference quantitatively, THz transmittance for all three samples is shown in Fig. 5(b). The transmittance drops by more than an order of magnitude within a sharply defined window between ∼0.3 and ∼1 THz (1 THz = 1 ps = 33.3 cm^{-1} = 4.1 meV) in agreement with Ref. [22]. The lower and upper cutoffs near 0.3 and 1 THz correspond to the slow and fast oscillations, respectively.

As mentioned earlier, $Sr_{14}Cu_{24}O_{41}$ has an IC structure with oppositely charged layers whose relative sliding motion gives rise to new gapped phonon modes. New IR modes were previously reported near 0.3 THz (lower cutoff) [22]. In the inelastic neutron scattering investigations, low-lying optical phonon modes were also revealed in the same energy range [23]. In Ref. [22], it was conjectured that these modes are due to the relative sliding motion of oppositely charged chain and ladder sheets. In the THz transmittance data of our as-grown crystal, we also see absorption modes near the lower cutoff in the frequency range 0.25–0.30 THz. To find out whether these modes are due to the sliding motion as conjectured earlier, we measured THz transmittance of an O_2-annealed crystal.

Interestingly, upon O_2 annealing, these modes merged to yield a sharper absorption band whose center shifted to a higher frequency near 0.35 THz. In the following, we argue that this dramatic stiffening is indeed consistent with the sliding motion scenario.

We recall that the degree of incommensurability in the IC systems depends sensitively on its stoichiometry [34]. In the present case, one can express the stoichiometry in terms of parameter α as $[CuO_2]_\alpha[Sr_2Cu_2O_3]$, where $\alpha = 10/7$ for an ideal formulation. However, as shown by Hiroi *et al.*, as-prepared $Sr_{14}Cu_{24}O_{41}$ samples exhibit a broad distribution of α values around the commensurate point $\alpha = 10/7$. Interestingly, by oxidizing or reducing the sample, the distribution width of α narrows considerably [19]. In other words, the as-prepared samples exhibit a high and varying degree of incommensurability, which can be reduced by annealing. We believe that oxygen annealing has a similar effect in our crystal, i.e., it reduces the degree of misfit between the chains and ladders, which results in the suppression of the excess specific heat associated with the sliding motion that results from this misfit. In the Appendix, we show C_p for several as-grown and annealed crystals. It is shown that unlike O_2 annealing, due to air annealing the excess C_p diminishes only negligibly, which reinforces the point that oxygen stoichiometry is important.

The effect of Al doping is more complex as it not only affects the oxygen stoichiometry as discussed next, but it also acts as a pinning center due to its different ionic radius and charge state compared to the host ion. In Ref. [31], it has been shown that the effect of Al-doping on $\chi(T)$ can only be correctly accounted for if one assumes that Al is doped in the ladder sheets. Since Al concentration is very small, to understand its effect on the sliding motion, we first consider the effect of Al doping on the oxygen stoichiometry. Since Al^{3+} replaces Cu^{2+} in the ladders, the charge neutrality requires an equivalent quantity of oxygen absorption by the sample unless some Cu^{2+} reduces to Cu^{1+}, which is unlikely due to an oxygen-rich crystal growth atmosphere; in that sense, the effect of Al doping is analogous to O_2 annealing. However, Al^{3+} impurities are also expected to *pin* the sliding density wave (DW) in a manner analogous to impurity pinning in charge and spin DW systems.

The other dominant effect of Al doping is on the upper cutoff of the transmittance near ~4 meV energy (1 THz), which shows a much higher sensitivity to Al doping compared to O_2 annealing. This can be understood by assuming that the upper cutoff in THz transmittance arises due to the charge density wave (CDW) ordering in the ladder sheets [35]. Since Al is doped in the ladders, its presence in the ladders probably perturbs the CDW ordering to some extent, resulting in a smearing of the upper cutoff. On the other hand, as shown by Hiroi *et al.* [19], oxygen annealing results in an increase in the number of free spins due to breaking of the dimers in the chains. Therefore, it is not expected to have any significant effect on the CDW ordering in the ladder sheets, which explains why the upper cutoff remains sharp and unshifted upon O_2 annealing. Further work to understand the role of impurities on the upper cutoff is currently in progress.

We now discuss the excess C_p near T^* and its subsequent suppression upon lightly doping or annealing the sample. The temperature variation of χ shows no anomalous feature around T^*, and it is well-fitted using the dimer-dimer model. This suggests a nonmagnetic or phononic origin of the excess C_p. This assignment of excess C_p is also consistent with the field-independent feature of ΔC_p. The conventional low-dimensional CDW systems [36], for example $K_{0.3}MoO_3$ [37] and $(TaSe_4)I$ [38], also show excess specific heat at low temperatures, but this arises due to the collective phase (phason) and amplitude (amplitudon) modes of the IC modulation below the CDW transition [16]. Though $Sr_{14}Cu_{24}O_{41}$ also undergoes a CDW ordering in the ladders below $T \approx 200$ K, the CDW in this case is not accompanied by a lattice distortion, and is believed to arise from the many-body electronic effects [39]. Therefore, a similar scenario as operative in conventional CDW systems seems inconceivable in the present case. Our experimental results suggest that the excess specific heat in $Sr_{14}Cu_{24}O_{41}$ arises from the relative sliding motion of the oppositely charged chain-ladder sheets, which is manifested in the form of THz modes near the lower cutoff of the transmittance window. The temperature $T^* = 10$ K of the peak in ΔC_p, and an almost exponential rate of decrease at lower temperatures, are consistent with a gapped scenario with a gap size close to 1 meV. C_p and THz of the annealed and Al-doped crystals also lend support to this interpretation. In the annealed sample, the peak in ΔC_p shifts to higher temperatures from ~10.5 to ~13.5 K, which is in agreement with the observed stiffening of the lower cutoff from ~0.28 THz (average ω for the as-grown crystal) to 0.35 THz upon oxygenation. In the case of the Al-doped sample, the stiffening of the lower cutoff is even more pronounced, which is not unexpected since Al impurities, besides changing the oxygen stoichiometry in a

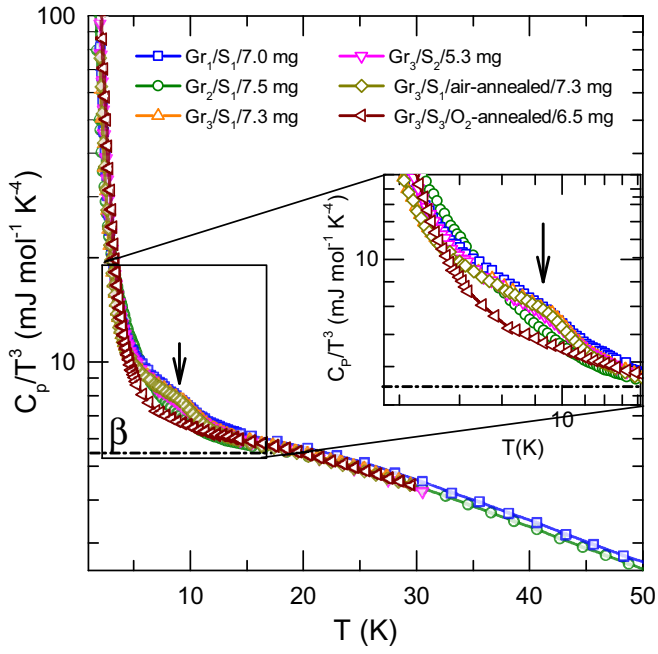

FIG. 6. Specific heat (C_p) of several as-grown single-crystalline specimens plotted as C_p/T^3 vs temperature (T). The excess specific heat is marked by an arrow. The dashed horizontal line corresponds to the βT^3 contribution of the three *acoustic* modes. A small variation in the magnitude of excess C_p between Gr_1S_1, Gr_2S_1, and Gr_3S_1 suggests that the excess C_p is highly sensitive to the stoichiometry as expected for an IC composite crystal.

manner analogous to O_2 annealing, also act as pinning centers impeding the sliding motion.

IV. CONCLUSIONS

To conclude, we showed the presence of a large excess specific heat in the IC chain-ladder compound $Sr_{14}Cu_{24}O_{41}$ around $T^* = 10$ K. However, no magnetic anomaly could be detected in the $\chi(T)$ data in this temperature range, which suggests that the excess C_p is of a nonmagnetic origin. The insensitivity of ΔC_p to the applied magnetic field further corroborates this conclusion. By using THz-TDS in the range from ~0.2 to ~1.4 THz, we argued that the excess C_p originates from the sliding phonon modes. Experiments on O_2-annealed and Al-doped crystals revealed significant suppression of the excess C_p, and concomitant changes in the THz response associated with the sliding modes. A very high sensitivity of the THz response to minor structural changes suggests that $Sr_{14}Cu_{24}O_{41}$ has a highly unconventional phononic ground state, which invites further investigations. Since Ca-doping at the Sr site in $Sr_{14}Cu_{24}O_{41}$ is known to transfer holes from chains to ladders, in the future it will be interesting to perform a systematic THz and specific heat study on variously Ca-doped $Sr_{14}Cu_{24}O_{41}$ samples.

APPENDIX

In Fig. 6, the specific heat (as-measured data) of several single crystalline specimens is shown in the low-temperature range. The samples are designated as G_iS_jm, where the subscript j refers to the jth specimen from the growth experiment labeled i. m is the mass of the sample measured in mg. The figure emphasizes small variations in C_p in the low-temperature range, which suggests that excess C_p is highly sensitive to the stoichiometry as expected for an IC composite crystal. In the O_2-annealed specimen, the excess C_p has diminished considerably, presumably due to a significant change of the oxygen stoichiometry. Interestingly, air-annealing at the same temperature and for the same duration has a negligible effect on C_p (see Gr_3S_1 and Gr_3S_1/air-annealed); this suggests that the excess C_p is suppressed due to a change in the oxygen stoichiometry rather than homogenization due to annealing.

[1] N. W. Ashcroft and N. D. Mermin, *Solid State Physics* (Saunders College, Philadelphia, 1976).
[2] J. D. Axe and P. Bak, Phys. Rev. B **26**, 4963 (1982).
[3] R. Zeyher and W. Finger, Phys. Rev. Lett. **49**, 1833 (1982).
[4] W. Finger and T. M. Rice, Phys. Rev. B **28**, 340 (1983).
[5] M. B. Walker and R. J. Gooding, Phys. Rev. B **32**, 7412 (1985).
[6] I. U. Heilmann, J. D. Axe, J. M. Hastings, G. Shirane, A. J. Heeger, and A. G. MacDiarmid, Phys. Rev. B **20**, 751 (1979).
[7] J. M. Hastings, J. P. Pouget, G. Shirane, A. J. Heeger, N. D. Miro, and A. G. MacDiarmid, Phys. Rev. Lett. **39**, 1484 (1977).
[8] X. Chen, A. Weathers, J. Carrete, S. Mukhopadhyay, O. Delaire, D. A. Stewart, N. Mingo, S. N. Girard, J. Ma, D. L. Abernathy, J. Yan, R. Sheshka, D. P. Sellan, F. Meng, S. Jin, J. Zhou, and L. Shi, Nat. Commun. **6**, 6723 (2015).
[9] I. Loa, L. F. Lundegaard, M. I. McMahon, S. R. Evans, A. Bossak, and M. Krisch, Phys. Rev. Lett. **99**, 035501 (2007).
[10] B. Toudic, R. Lefort, C. Ecolivet, L. Guérin, R. Currat, P. Bourges, and T. Breczewski, Phys. Rev. Lett. **107**, 205502 (2011).
[11] J. Etrillard, P. Bourges, H. F. He, B. Keimer, B. Liang, and C. T. Lin, Europhys. Lett. **55**, 201 (2001).
[12] J. Etrillard, L. Bourgeois, P. Bourges, B. Liang, C. T. Lin, and B. Keimer, Europhys. Lett. **66**, 246 (2004).
[13] G. Theodorou and T. M. Rice, Phys. Rev. B **18**, 2840 (1978).
[14] J. Etrillard, J. C. Lasjaunias, K. Biljakovic, B. Toudic, and G. Coddens, Phys. Rev. Lett. **76**, 2334 (1996).
[15] A. Cano and A. P. Levanyuk, Phys. Rev. Lett. **93**, 245902 (2004).
[16] G. Reményi, S. Sahling, K. Biljaković, D. Starešinić, J.-C. Lasjaunias, J. E. Lorenzo, P. Monceau, and A. Cano, Phys. Rev. Lett. **114**, 195502 (2015).
[17] C. H. Lee, I. Hase, H. Sugawara, H. Yoshizawa, and H. Sato, J. Phys. Soc. Jpn. **75**, 123602 (2006).
[18] P. Brown, K. Semeniuk, D. Wang, B. Monserrat, C. J. Pickard, and F. M. Grosche, Sci. Adv. **4**, eaao4793 (2018).
[19] Z. Hiroi, S. Amelinckx, G. Van Tendeloo, and N. Kobayashi, Phys. Rev. B **54**, 15849 (1996).
[20] M. v. Zimmermann, J. Geck, S. Kiele, R. Klingeler, and B. Büchner, Phys. Rev. B **73**, 115121 (2006).
[21] E. Dagotto, Rep. Prog. Phys. **62**, 1525 (1999).
[22] V. K. Thorsmølle, C. C. Homes, A. Gozar, G. Blumberg, J. L. M. van Mechelen, A. B. Kuzmenko, S. Vanishri, C. Marin, and H. M. Rønnow, Phys. Rev. Lett. **108**, 217401 (2012).
[23] X. Chen, D. Bansal, S. Sullivan, D. L. Abernathy, A. A. Aczel, J. Zhou, O. Delaire, and L. Shi, Phys. Rev. B **94**, 134309 (2016).
[24] R. Bag, K. Karmakar, and S. Singh, J. Cryst. Growth **458**, 16 (2017).
[25] K. Magishi, S. Matsumoto, Y. Kitaoka, K. Ishida, K. Asayama, M. Uehara, T. Nagata, and J. Akimitsu, Phys. Rev. B **57**, 11533 (1998).
[26] R. S. Eccleston, M. Uehara, J. Akimitsu, H. Eisaki, N. Motoyama, and S.-i. Uchida, Phys. Rev. Lett. **81**, 1702 (1998).
[27] M. Takigawa, N. Motoyama, H. Eisaki, and S. Uchida, Phys. Rev. B **57**, 1124 (1998).
[28] F. C. Zhang and T. M. Rice, Phys. Rev. B **37**, 3759 (1988).
[29] S. Sahling, G. Remenyi, C. Paulsen, P. Monceau, V. Saligrama, C. Marin, A. Revcolevschi, L. P. Regnault, S. Raymond, and J. E. Lorenzo, Nat. Phys. **11**, 255 (2015).
[30] R. Klingeler, B. Büchner, K.-Y. Choi, V. Kataev, U. Ammerahl, A. Revcolevschi, and J. Schnack, Phys. Rev. B **73**, 014426 (2006).
[31] R. Bag, K. Karmakar, S. Dhar, M. Tripathi, R. J. Choudhary, and S. Singh, J. Phys.: Condens. Matter **31**, 035801 (2018).
[32] M. W. McElfresh, J. M. D. Coey, P. Strobel, and S. von Molnar, Phys. Rev. B **40**, 825 (1989).
[33] B. C. Melot, R. Tackett, J. O'Brien, A. L. Hector, G. Lawes, R. Seshadri, and A. P. Ramirez, Phys. Rev. B **79**, 224111 (2009).
[34] S. V. Smaalen, Crystallogr. Rev. **4**, 79 (1995).

[35] G. Blumberg, P. Littlewood, A. Gozar, B. S. Dennis, N. Motoyama, H. Eisaki, and S. Uchida, Science **297**, 584 (2002).

[36] G. Grüner, *Density Waves in Solids*, Advanced Book Program (Addison-Wesley, Reading, MA, 2000).

[37] J. Odin, J. Lasjaunias, K. Biljaković, K. Hasselbach, and P. Monceau, Eur. Phys. J. B **24**, 315 (2001).

[38] K. Biljakovic, J. C. Lasjaunias, F. Zougmore, P. Monceau, F. Levy, L. Bernard, and R. Currat, Phys. Rev. Lett. **57**, 1907 (1986).

[39] P. Abbamonte, G. Blumberg, A. Rusydi, A. Gozar, P. G. Evans, T. Siegrist, L. Venema, H. Eisaki, E. D. Isaacs, and G. A. Sawatzky, Nature (London) **431**, 1078 (2004).